

THE AES40 NORTH ATLANTIC WAVE REANALYSIS: VALIDATION AND CLIMATE ASSESSMENT

V.R Swail¹, E.A Ceccacci² and A.T. Cox²

¹Environment Canada
Downsview, Ontario

²Oceanweather, Inc.
Cos Cob, CT

1. INTRODUCTION

The advent of long-term climate reanalysis projects undertaken by major numerical weather prediction centres has significantly changed the approach to the investigation of climate variability and trend on decadal and longer time scales. Swail and Cox (2000) evaluated the suitability of the NCEP-NCAR Reanalysis Project (NRA) wind fields to generate a long-term wave hindcast of the North Atlantic Ocean (NA). Swail *et al.* (1998) described in detail a project undertaken by Oceanweather Inc. for the Meteorological Service of Canada (formerly Atmospheric Environment Service (AES)) to produce the first 40-year (1958-1997) wind and wave hindcast of the North Atlantic (AES40). The objective of the study was to use the NRA products (Kalnay *et al.*, 1996) to drive a third-generation wave model adapted to the NA on a high-resolution grid to produce a high-quality, homogeneous, long term wind and wave data base for assessment of the wave climate of the NA, its trend and variability. The most important feature of the hindcast was the rigorous attention devoted to producing the wind fields used to drive the wave model. To remove potential biases in the historical wind fields, all wind observations from ships and buoys were re-assimilated into the analysis taking account of the method of observation, anemometer height and stability. Wind fields for all significant storms were then painstakingly kinematically reanalyzed with the aid of an interactive Wind Workstation (Cox *et al.*, 1995). Furthermore, high-resolution surface wind fields for all tropical cyclones, as specified by a proven tropical cyclone boundary layer model, were assimilated into the wind fields to provide greater skill and resolution in the resulting wave hindcasts.

This paper describes the validation of the AES40 hindcast wind and wave fields, and analysis of the wave climate, its trend and variability. The wave model is described in Section 2. The generation of the homogeneous, high-quality wind fields used as input to the wave model is described in detail in Section 3.

Section 4 describes the extensive evaluation of the model winds and waves compared to both *in situ* and satellite observations. Finally, Section 5 shows results of the climate assessment, including both engineering-type analyses and climate trend analysis.

2. WAVE MODEL

The wave model used for this hindcast is a discrete spectral type called OWI 3-G. The spectrum is resolved at each grid point in 24 directional bins and 23 frequency bins. The bin centre frequencies range from 0.039 Hz to 0.32 Hz increasing in geometric progression with a constant ratio 1.10064. Deep-water physics is assumed in both the propagation algorithm and the source terms. The propagation scheme (Greenwood *et al.*, 1985) is a downstream interpolatory scheme that is rigorously energy conserving with great circle propagation effects included. The source term formulation and integration is a third-generation type (WAMDI, 1988) but with different numerics and with the following modifications of the source terms in official WAMDI. First, a linear excitation source term is added to the input source term to allow the sea to grow from a flat calm condition without an artificial warm start sea state. The exponential wind input source is taken as the Snyder *et al.* (1981) linear function of friction velocity, as in WAMDI. However, unlike WAM, in which friction velocity is computed from the input 10-m wind speed following the drag law of Wu (1982), a different drag law is used in OWI 3-G. That law follows Wu closely up to wind speed of 20 m/s and then becomes asymptotic to a constant at hurricane wind speeds. The dissipation source term is taken from WAMDI except that the frequency dependence is cubic rather than quadratic. Finally, the discrete interaction approximation to the non-linear source term is used as in WAMDI except that two modes of interaction are included (in WAMDI the second mode is ignored). Further details on this model and its validation may be found in Khandekar *et al.* (1994), Cardone *et al.* (1996) and Forristall and Greenwood (1998). This wave model has been shown to reproduce observed wave heights

very well when driven by accurate wind fields (Cardone *et al.*, 1995, 1996).

OWI 3-G is adapted on a latitude-longitude grid consisting of a 122 (in latitude) by 126 (in longitude) array of points. The grid spacing is 0.625° in latitude by 0.833° in longitude, which is within 10% of square (i.e. $\Delta x = \Delta y$) between 38° and 45° N. The eastern boundary is at 20° E longitude and the northern boundary is at 75.625° N latitude. After deductions for land there are 9023 grid points. The south edge of the grid is at the equator. This boundary was treated as open; wave spectra interpolated from the output of a lower resolution (2.5 degrees at a 3-hour time step) global second generation model driven by unmodified NRA 10 m wind fields (Cox and Swail, 2000) are used as boundary conditions along the equator to preserve any South Atlantic swells. The basic model integration time step is 0.5 hours and consists of one 30 minute propagation time step and two 15 minute growth cycles.

The hindcast was carried out in monthly segments using the OWI 3-G wave model in deep water mode driven by the final kinematically reanalyzed wind fields as described in the next section. A spectral save file was generated at the end of each month of integration and used to initialize the spectrum for the run of the succeeding month (warm start). Ice cover was specified for each month from mid-monthly ice tables specified on the wave grid from Walsh & Johnson (1979) (prior to 1972), Arctic and Antarctic Sea Ice Data CD-ROM 1972-1994, and hand-digitized maps produced from the joint Navy/NOAA Ice Center data sets. The 5/10-ice concentration contour was used as the definition of the ice edge - points with ice concentrations greater than 5/10 were considered as land by the model, those with concentrations 5/10 or less were considered as open water. The output of the model consists of 17 'fields' quantities (e.g. significant wave height, peak period, vector mean direction, partitioned fields, directional and angular spreading) at all grid points and the full two-dimensional spectrum at 233 grid points. The spectral save points were selected to allow even coverage of the basin (every 5° of latitude and longitude), as well as to allow the possibility to drive finer mesh models for the US East Coast, the Scotian Shelf and Grand Banks of Newfoundland and the European West Coast. Spectra were also saved at the locations of selected moored buoys and offshore platforms.

3. WIND FIELDS

The most important, and unique, element of the AES40 hindcast was the enormous effort devoted to producing the wind fields for the wave model; this effort accounted for more than 10,000 meteorologist-hours of effort spent in manual and interactive kinematic analysis. Details of the wind field generation are given in Swail and Cox (2000); however, a brief description will be included here for completeness.

In the first step of the wind field generation, NRA surface (10 m) winds are brought into the Wind WorkStation every 6 hours in monthly segments, after first being converted to an equivalent neutral wind using the NRA 2 m surface temperature and sea-surface temperature fields and the algorithm described by Cardone *et al.* (1990).

In the second step of the wind analysis, all available historical marine surface data, including buoy observations, ship reports, coastal stations and ERS 1/2 scatterometer winds are displayed in the Wind WorkStation. A crucial feature of the AES40 hindcast concerns the treatment of these surface observations. The NRA assimilation scheme (as with most numerical weather prediction schemes) treated all observations at a 10 m reference level, whereas ship and drilling platform observations may actually range from about 15 m to more than 100 m, and buoy observations are typically taken about 5 m. Over the 40 year duration of the NRA this may introduce biases similar to those found by Cardone *et al.* (1990) due to the increasing heights of shipboard anemometers and the higher fraction of wind measurements compared to wind estimates. To overcome any potential bias in this project, all surface wind data were first adjusted to effective neutral 10-m winds.

It was found in the NRA hindcasts that tropical storms are poorly resolved in the NRA wind fields. In the third step of the wind analysis, high resolution surface wind fields for all tropical cyclones, as specified by a proven tropical cyclone boundary layer model (Cardone *et al.*, 1994; Thompson and Cardone, 1996), are assimilated into the wind fields to provide greater skill and resolution in the resulting wave hindcasts. Track and initial estimates of intensity are taken, with some modification, from the NOAA Tropical Prediction Center's (TPC) HURDAT database. The radius of maximum wind is determined using a pressure profile fit to available surface observations and aircraft reconnaissance data. Reconnaissance data are taken from TPC's Annual Data and Verification Tabulation diskettes from 1989-1996, digitally scanned from manuscript records for the period 1974-1988, and

manually scanned from reconnaissance microfilm for periods prior to 1974. Surface winds generated from the model are then evaluated against available surface data and aircraft reconnaissance wind observations adjusted to the surface as described by Powell *et al.* (1989). Model winds within 240 nautical miles from the centre are then exported on a 0.5° latitude-longitude grid for inclusion and blending using the Wind WorkStation.

The fourth, and most labour-intensive and time-consuming, but also the most important step, was the detailed kinematic analysis incorporating all of the wind information noted above. The interactive wind analysis methodology used follows similar previous hindcast studies (Cardone *et al.*, 1995, 1996). Particular attention is spent on strong extra-tropical systems, blending tropical model winds into the NCEP surface wind field, and in the quality control of surface data. Kinematically analyzed winds from previous hindcasts of severe extratropical storms in the northwest Atlantic (Swail *et al.*, 1995) are incorporated into the present analysis on the North Atlantic wave model grid.

Altimeter wave measurements are used in an inverse modelling approach as follows. Hindcast wave heights over the North Atlantic Ocean derived from the global 2-G model described in Section 2 are compared to altimeter wave measurements. Areas where the resulting wave fields are deficient, as indicated by the altimeter, are brought to the analysts' attention and the analyst subjectively rectifies the deficiencies in the backward space-time evolution of the NRA wind field causing the discrepancy.

Final wind fields for each month were interpolated onto the 0.625° by 0.833° latitude-longitude wave model grid using the IOKA (Interactive Objective Kinematic Analysis) algorithm (Cox *et al.*, 1995) and then time interpolated to a one-hour time step.

4. VALIDATION

4.1 Validation Data Sets

4.1.1. Buoys and Platforms

The *in situ* validation data set included buoys and measurement platforms mainly located along the continental margins. The *in situ* measured wind and wave data came from a variety of sources. U.S. buoy data came from the NOAA Marine Environmental Buoy Database on CD-ROM; the Canadian buoy data came from the Marine Environmental Data Service marine CD-ROM; the remaining buoy and platform

data (notably the northeast Atlantic) came from the Comprehensive Ocean Atmosphere Data Set (COADS) data set described by Slutz *et al.* (1985). Comparisons were restricted to well-exposed deep-water sites with the longest records. The wave measurements are comprised of 20-minute samples (except for Canadian buoys which were 40 minutes) once per hour. The wind measurements were taken as 10-minute samples, scalar averaged, except vector averaged at the Canadian buoys, also once per hour. The wind and wave values selected for comparison with the hindcast were 3-hour mean values centered on each six-hour synoptic time with equal (1,1,1) weighting. All wind speeds were adjusted to 10-m neutral winds following the approach described in Cardone *et al.* (1990).

4.1.2. Satellite Data

Altimeters from the ERS-1, ERS-2 and TOPEX/Poseidon instruments were used for wind and wave comparisons. The ERS-1/2 altimeter data sets were obtained from the Ifremer CD-ROM data set, while TOPEX data (GDR Generation-B CD-ROM set) was obtained from the NASA Physical Oceanography Distributed Active Archive Center at the Jet Propulsion Laboratory/California Institute of Technology. Both data sets were decoded using the recommended quality controls described in each respective documentation. Further adjustments and quality control measures were used as recommended by Cotton and Carter (1994) to make the observations from differing platforms consistent with each other. Individual data points were then spatially binned onto the wave model grid, and output on to 6-hour synoptic times using a ± 3 -hour window. Additional quality control was performed for measurements along land and ice edges where some contamination of the altimeter wave measurements was encountered despite rigorous checking of ice/quality control flags available with each data set.

4.2 *In situ* Comparisons

Individual buoys and platforms were grouped by region for comparison against the AES40 hindcast. Table 1 shows regional grouped statistics and represents more than 200,000 wind and wave observations. Highest scatter indices (SI) are from the northeast Atlantic regions, which were made up exclusively of COADS data. The COADS data lacks both the time resolution (3/6 hours versus 1 hour) and coding accuracy (winds nearest 1 knot, waves 0.5 m) than the other regions obtained from the CD-ROM marine data sets, which may explain some of the differences in SI. The Canadian and U.S. buoys were grouped into one data set since they represented the best science quality validation data set. These statistics show very good

agreement with a mean bias of 0.31 m/s for winds and 0.10 m for waves and SI of 0.23 for both winds and waves. Wind speed scatter at the Canadian buoys is

high, 0.31, mainly due to questionable data from one buoy which was left out in the wind assimilation but left in the comparisons shown here.

Table 1. Regional statistical comparison of AES40 vs. *in situ* buoy and platform observations.

	Number of Points	Mean Meas	Mean Hind	Diff (H-M)	RMS Error	Std. Dev.	Scatter Index	Corr. Coeff.
<i>U.S. Buoys</i>								
Ws (m/s)	169927	6.92	7.18	0.26	1.31	1.28	0.19	0.94
Wd (°)	169925	240.47	251.65	0.99	N/A	16.65	0.05	N/A
Hs (m)	164834	1.83	1.94	0.12	0.43	0.42	0.23	0.93
<i>Canadian Buoys</i>								
Ws (m/s)	49272	7.94	8.41	0.46	2.54	2.50	0.31	0.84
Wd (°)	49272	263.46	268.87	1.58	N/A	29.48	0.08	N/A
Hs (m)	48890	2.51	2.53	0.03	0.53	0.53	0.21	0.93
<i>East Atlantic Buoys</i>								
Ws (m/s)	11019	9.75	9.71	-0.04	1.64	1.64	0.17	0.93
Wd (°)	11027	245.40	244.27	-0.44	N/A	17.98	0.05	N/A
Hs (m)	8071	3.73	3.47	-0.27	1.68	1.65	0.44	0.74
<i>North/Norwegian Sea Platforms and Buoys</i>								
Ws (m/s)	117198	8.58	9.14	0.56	2.24	2.17	0.25	0.88
Wd (°)	117204	240.17	239.27	-1.09	N/A	22.64	0.06	N/A
Hs (m)	107301	2.47	2.67	0.20	0.96	0.94	0.38	0.83
<i>U.S. and Canadian Data Combined</i>								
Ws (m/s)	219199	7.15	7.45	0.31	1.67	1.64	0.23	0.91
Wd (°)	219197	247.72	257.67	1.11	N/A	20.14	0.06	N/A
Hs (m)	213724	1.98	2.08	0.10	0.46	0.45	0.23	0.93

A quantile-quantile comparison of wind speed and wave height for the combined U.S. and Canadian buoys (Figure 1) shows excellent agreement from the 1st to 99th percentile. There is a small overestimation of both the winds and waves (mean difference is 0.31 m/s and 0.10 meters), however the near-linear comparison indicates that AES40 is properly describing the wind and wave climate at the buoy locations up to and including the 99th percentile.

While overall statistics are useful for evaluating the skill of a hindcast, they don't indicate how the hindcast has changed over time relative to the *in situ* data. A comparison of seasonal wave height bias and scatter over the 1975-1997 period (Figure 2) shows any trends that may exist in the hindcasts. Of course, trends may also occur in the measurements themselves (number of observations available, differing instrumentation, etc.) and the measured data must be evaluated carefully. These plots were produced by computing bias and SI

for each region for every 3 months and plotting the resulting time series. Figure 2 shows good agreement between the buoy observations and AES40 over time. The plots show nearly linear bias and SI over time indicating that AES40 has remained consistent over the 22 years that the buoy measurements are available. Highest SI values occur in the data from COADS, while the US and Canadian comparisons are more consistent. Early US buoy comparisons show more bias and slightly higher SI, which may be due to the relatively few experimental buoys available in late 70's/early 80's.

4.3 Satellite Comparisons

Altimeter wind and wave measurements provide the best spatial coverage to evaluate wave hindcasts. Statistics and plots from the individual instruments (ERS-1, ERS-2, and TOPEX) showed very good agreement between each other, so the data sets were

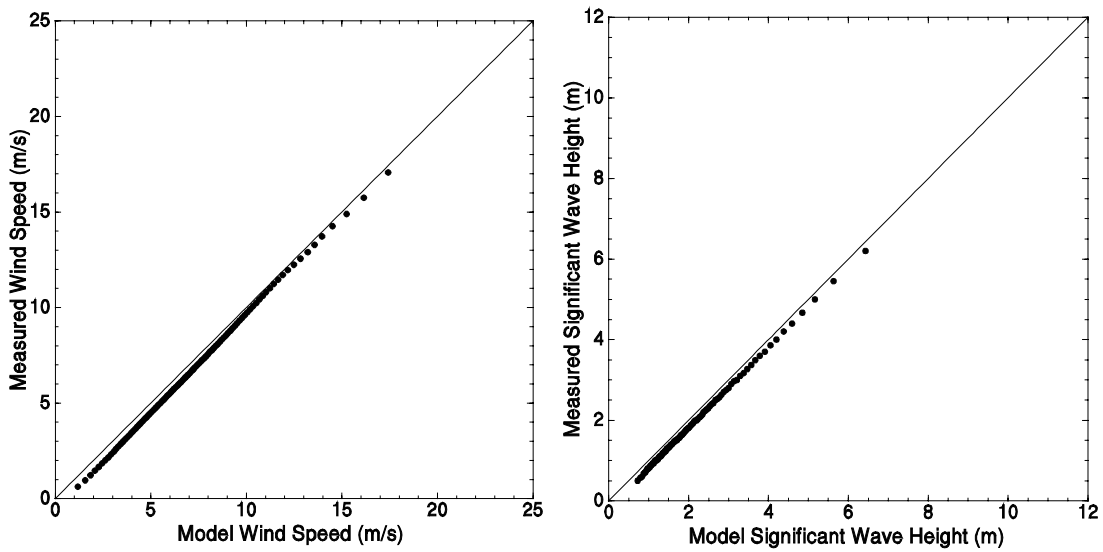


Figure 1. Quantile-Quantile comparison from 1 to 99% for combined U.S. and Canadian buoys vs. AES40 wind speed (m/s, left) and significant wave height (meters, right).

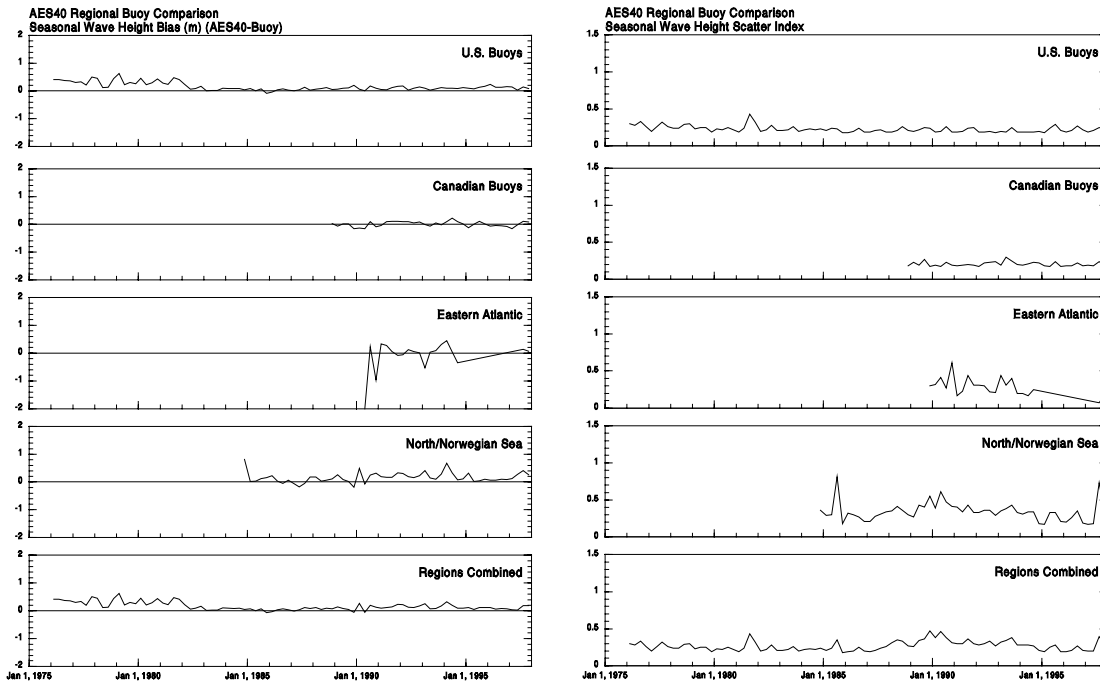


Figure 2. Seasonal wave height bias (m) (left) and scatter (right) comparison of AES40 vs. buoys by region

combined for these comparisons. Comparisons were done for the full basin only. Statistics are summarized in Table 2. The wave height comparisons showed near-zero bias, while the model winds were slightly higher

than the satellite values. Scatter indices were of comparable magnitude to the *in situ* comparisons.

Table 2. Regional statistical comparison of AES40 vs. altimeter measurements.

	Number of Points	Mean Meas	Mean Hind	Diff (H-M)	RMS Error	Std. Dev.	Scatter Index	Corr. Coeff.
Ws (m/s)	3471109	7.66	7.81	0.15	1.94	1.94	0.25	0.86
Hs (m)	3523575	2.52	2.51	-0.01	0.56	0.56	0.22	0.93

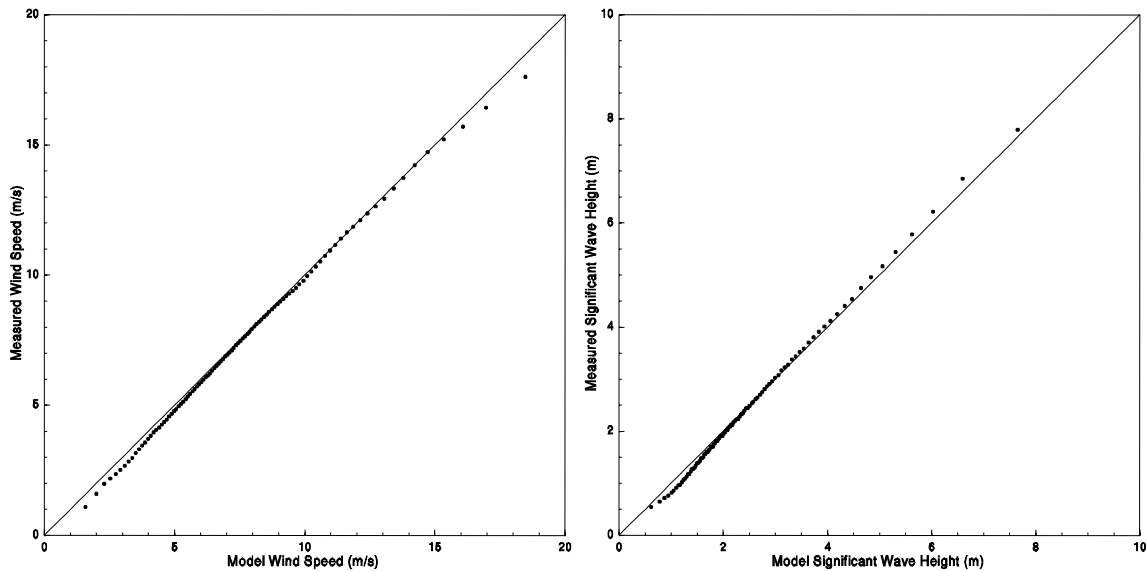


Figure 3. Q-Q wind speed (m/s) and wave height (m) comparisons of AES40 and altimeter measurements.

Quantile-quantile (Q-Q) plots of the combined altimeter versus AES40 (Figure 3) show excellent agreement for both wind speed and wave height. At the highest percentiles, winds appear to be over-predicted while waves track up to the 99th percentile. This is suspected to be a wind speed saturation problem with the altimeter in wind speeds above 15 m/s.

The extensive coverage of the altimeter measurements makes it possible to plot contours of wave bias on a basin-wide projection. A spatial wave bias plot of AES40 (Figure 4) shows that over most of the North Atlantic AES40 has very little bias. The largest feature is the underestimation in Baffin Bay and in the Denmark Strait. This is suspected to be a result of ice edge effects, and to some degree an underestimation of the wind speed in the NRA winds. While the AES40 winds were kinematically enhanced, the lack of data in these areas made it

difficult to track all significant systems. When sufficient data were available, large discrepancies of the wind speed were found and corrected in the NRA winds. Grid scale effects explain most other areas of bias near island chains or in the shallow Southern North Sea.

A basin map of wave height scatter index (SI) (Figure 5) shows many of the same patterns as the wave height bias map. In general, the SI is very small (near or under .20 for most of the basin) with larger values at the coasts and along water/ice boundaries.

All Combined (ERS-1,ERS-2,TOPEX) Altimeter/AES40 Comparison
Mean Difference of Significant Wave Height (m) AES40-ALTIMETER

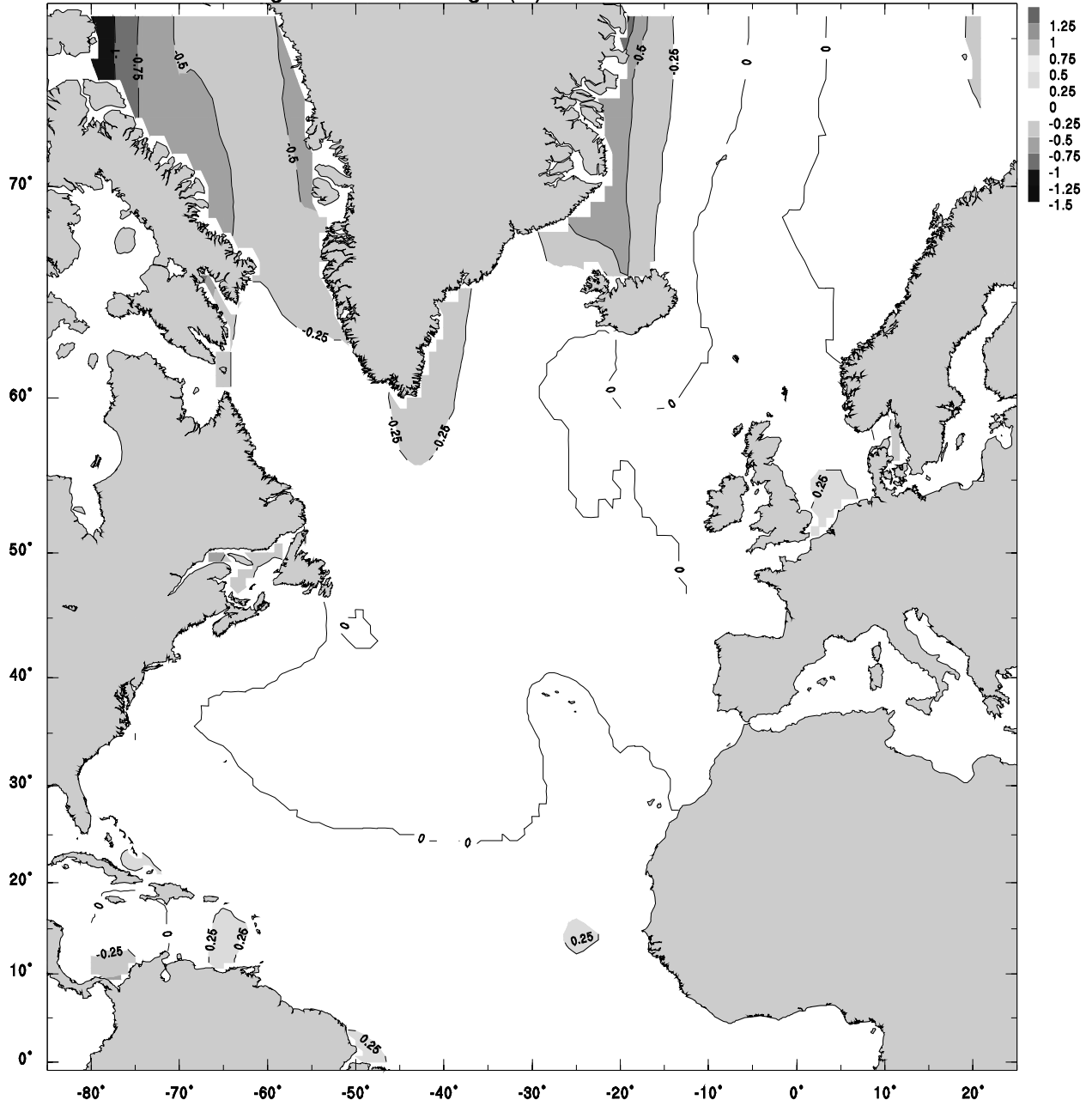


Figure 4. Mean difference of wave height (m) between AES40 and altimeter measurements (AES40-Altimeter)

Combined (ERS-1,ERS-2,TOPEX) Altimeter/AES40 Comparison
Scatter Index of Significant Wave Height (m)

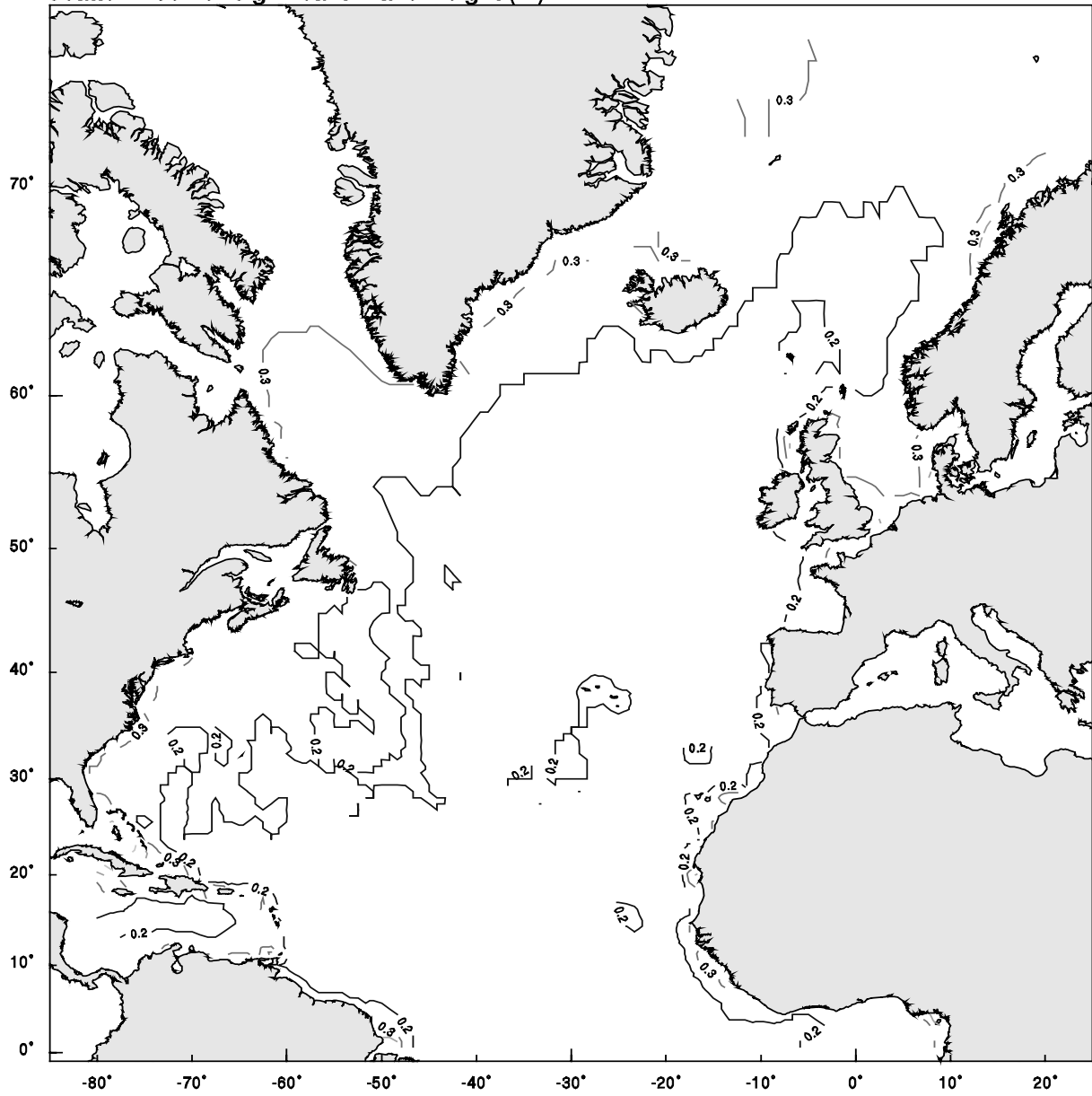


Figure 5. Comparison of wave height scatter index (RMS/Mean Altimeter) for combined ERS 1/2 and TOPEX wave measurements vs. AES40 for period 1991-1997.

5. CLIMATE ASSESSMENT

5.1 Trend and Variability Analysis

Fifteen statistics were computed for both the input wind fields and resultant wave heights on monthly,

seasonal and annual time scales; trend and variability analysis was carried out for every grid point in the hindcast. Among the statistics computed were: mean, standard deviation, skew, kurtosis, 50th, 90th, 95 and 99th percentiles, and exceedance above selected thresholds.

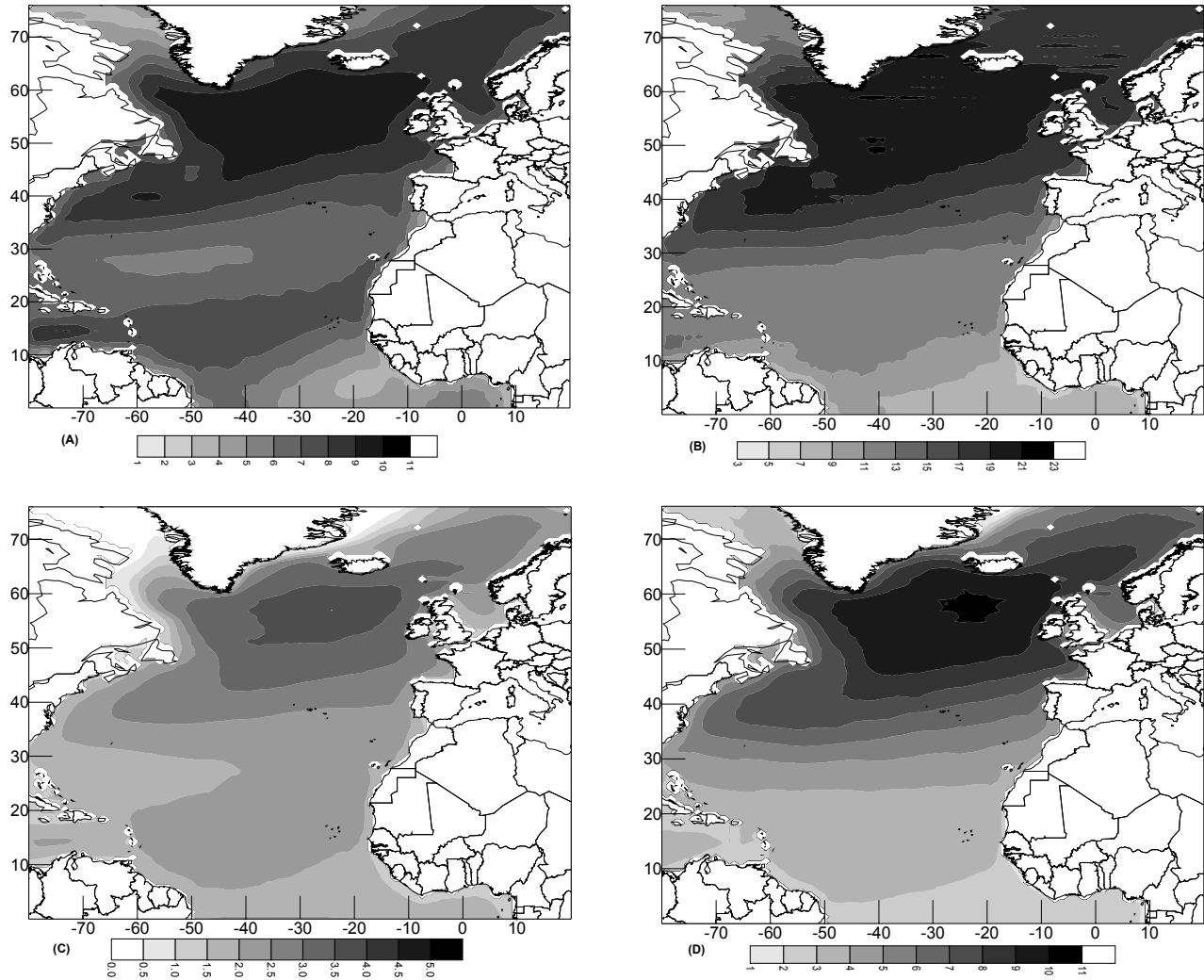


Figure 6. Wind speed and wave height statistics over the period 1958-1997: (a) annual mean wind speed; (b) 99th percentile wind speed; (c) annual mean wave height; (d) 99th percentile wave height

Figure 6 (a,b) shows the mean annual wind speed and wave height distribution for the period 1958 to 1997. The maxima in the high latitude areas and along the prevailing storm tracks are very evident in these charts.

Figure 6 (c,d) shows the geographical distribution of the annual 99th percentile wind speed and wave height for 1958-1997. The patterns are very similar to those for the means, although the areas of highest

wind speed and wave height are even more accentuated.

A series of statistical analyses of the wind and wave trends was carried out at each grid point. Trends were computed as simple linear trends over the 40 years of the hindcast using least squares fitting techniques; 99% statistical significance levels were also computed. Figure 7 shows the trends in the mean and 99th percentile wind speed and wave heights; trends are expressed as the inferred change over the 40-year

period 1958-1997 based on the slope of the linear trend line. Increasing trends are most noticeable in the northeast Atlantic Ocean. Negative trends in wave height are found in the Labrador Sea. Particularly noticeable is the bi-polar nature of the trends in the North Atlantic, with strong increases in the northeast, and strong decreases in the south

central North Atlantic. This pattern follows the dominant mode of the North Atlantic Oscillation. The trends are much more pronounced for the extreme wave heights (99th percentile) than for the mean conditions, with large areas of increases of wave height more than 1 m.

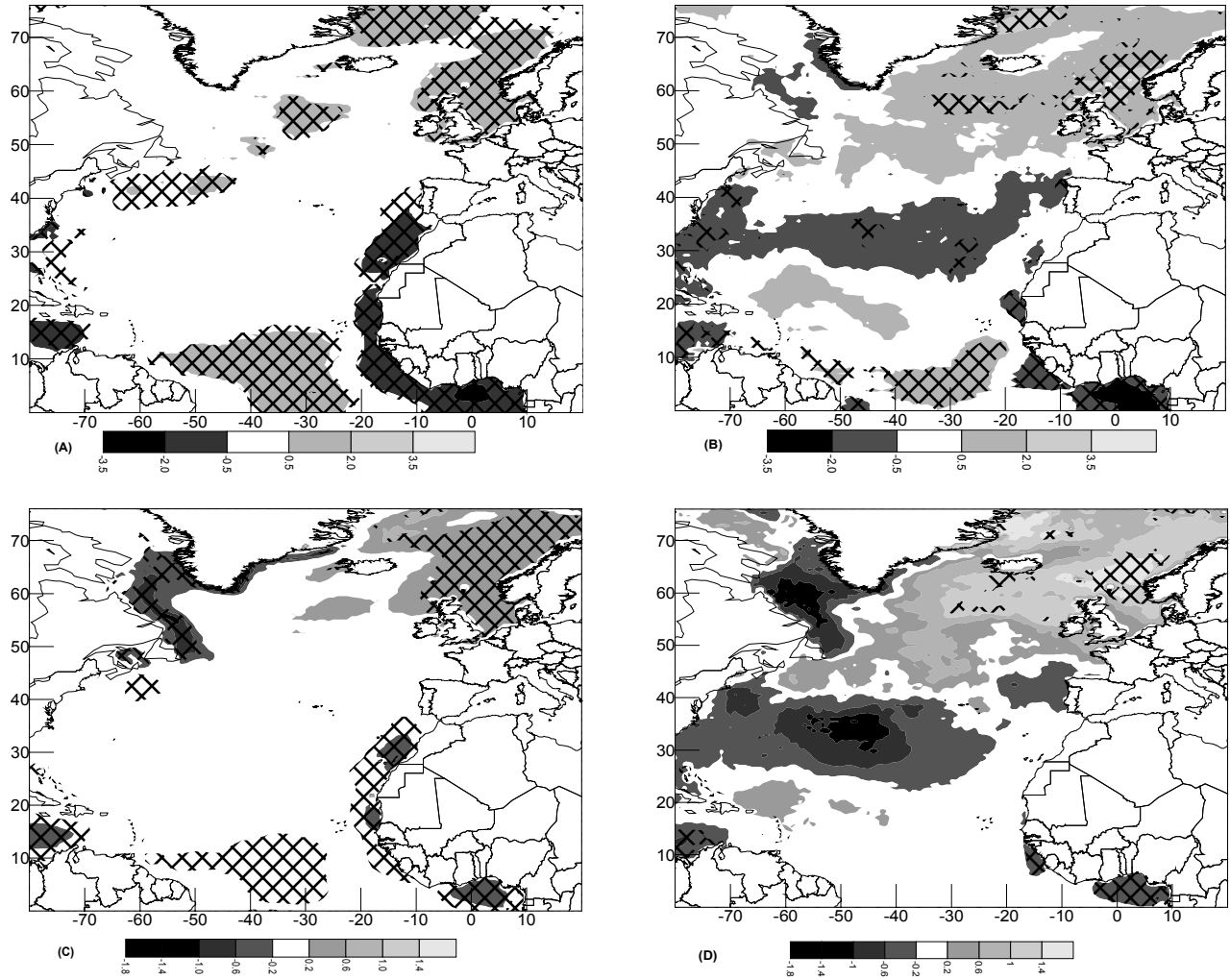


Figure 7. Inferred change over the period 1958-1997 with 99% statistical significance in (a) annual mean wind speed; (b) 99th percentile wind speed; (c) annual mean wave height; (d) 99th percentile wave height

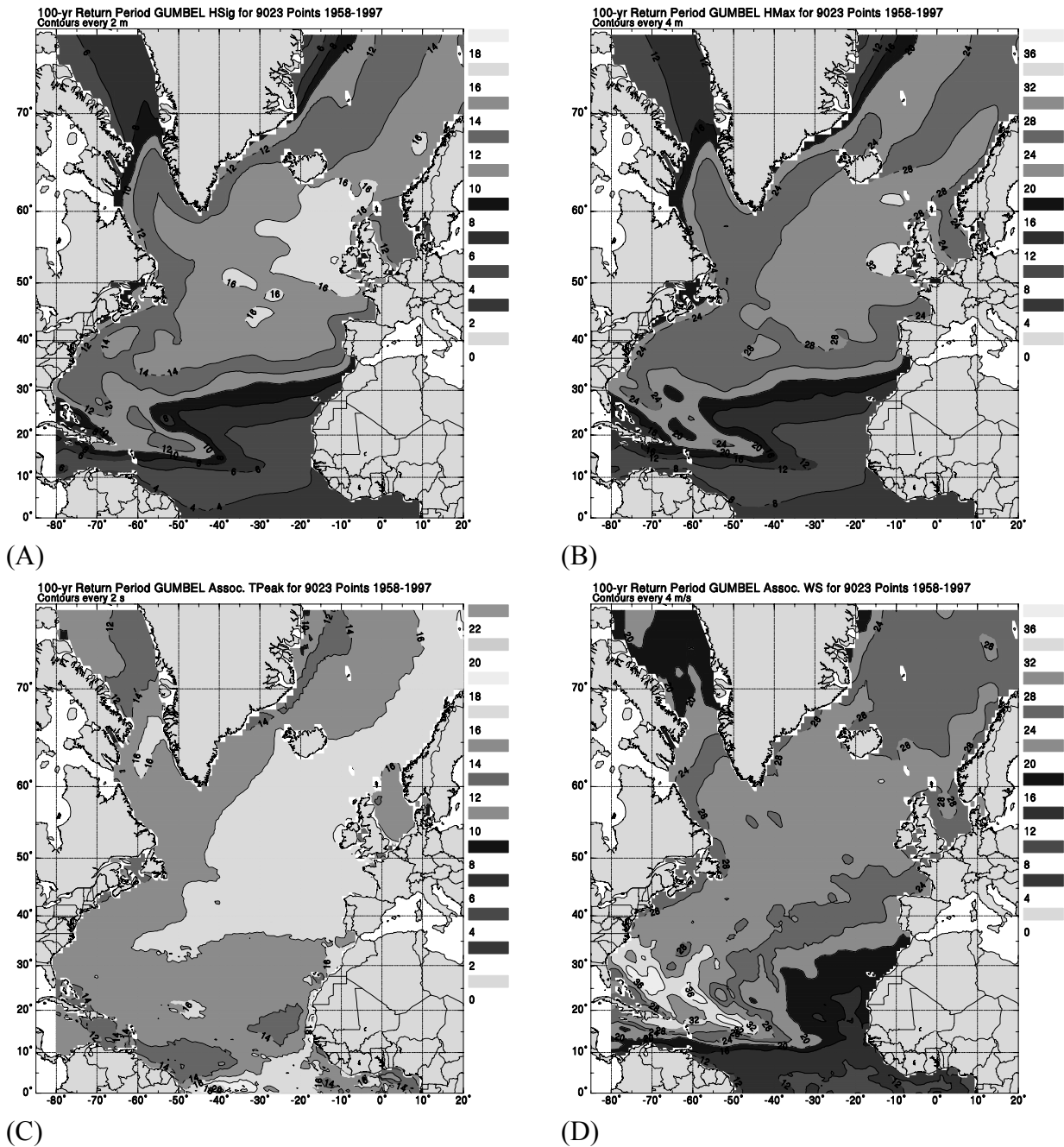


Figure 8. 100-year return period statistics for AES40 hindcast 1958-1997. All peaks combined. Gumbel analysis. (A) significant wave height; contours every 2 m; (B) maximum wave height, contours every 4 m; (C) peak period associated, contours every 2 s; (D) wind speed associated, contours every 4 m/s

5.2 Extreme Value Analysis

Three populations of storms were used for the extremal analysis. "Tropical" refers to any peak which occurred within 240 nmi of a tropical system center location at any intensity. "Extratropical" refers to any peak that is not considered "Tropical." Finally, "combined" contains every peak. A peak is defined as any event that greater than the minimum significant wave height threshold, and must be separated from any other peak by at least 48 hours. The length of a storm for the maximum wave and crest computations is defined as the time when significant wave height is greater than one-half of the peak of that particular event, or a maximum of 48-hours, where the peak is at the midpoint. The minimum significant wave height threshold varied with latitude, 2.5 m from 0-31.25°N and 3.0 m from 31.25°N-75.625°N. For locations covered often by ice and very sheltered locations along the African coast, a lower threshold of 0.5 m was used to achieve a minimum of 4 peaks.

Peaks were produced for seven time slices: 1958-1997 (all 40 years); 1958-1977 and 1978-1997; 1958-1967, 1968-1977, 1978-1987, and 1988-1997. All peaks were processed using two extremal distributions, Gumbel and Weibull (Borgman, 1973; Forristall, 1978; Gumbel, 1958; Haring *et al.*, 1976). In each case, the top 40 peaks (with a minimum of four peaks) were used to produce a fit at each of the 9023 grid points. Seven return periods were computed: 2, 5, 10, 20, 40, 50, and 100 years for each of the following six variables: significant wave height (SWH), maximum wave, maximum crest, peak period (associated with SWH), wind speed that occurred at the same time as SWH, and maximum wind speed (can occur independently of SWH but within the storm length as defined above). Figure 8 shows the 100-year Gumbel analysis of the entire 40-year period for significant and maximum wave height, associated wind speed and peak period; the wave height and wind speed contours were smoothed using an evenly weighted 9-point average. Unsmoothed SWH values were used to develop the regression analysis for peak period, but smoothed values were used to derive the associated peak period values shown in the figure.

From Figure 8 it can be seen that the highest wind and wave conditions are expected to occur west of the United Kingdom and south of Iceland. Also, tropical system "trails" can be seen extending along 15-20°N and towards the northwest to the southern U.S. The other time slices showed similar results (not

shown) and were dictated by the relative storminess. The tropical system "trail" would grow or shrink accordingly as would the strongest area over the North East Atlantic. In fact, the strong North East Atlantic area shifted to the south and west and was centered along 50°N during the first and most recent decades.

5.3 Redundancy Analysis

Like canonical correlation analysis (CCA), redundancy analysis is a technique that is used to associate patterns of variation in a predictor field with patterns of the predictand field through a regression model. It differs from CCA because it seeks to find pairs of predictor and predictand patterns that maximize the associated predictand variance, rather than the correlation only. Redundancy analysis techniques (described by Wang *et al.*, 1999) were used to carry out detailed seasonal spatial statistical analyses. Significant increases in the northeast Atlantic in the 90th and 99th percentile wave heights were matched by significant decreases in the subtropical North Atlantic, for the winter (JFM) season. Linear trends detected for the 99th percentiles are generally less significant than those for the 90th percentiles. The correlation between sea level pressure (SLP) and the 90th percentile wave height (H90) is significant at the 99th confidence level. Both time series possess a significant increasing trend at the 95% confidence level, indicating that the Icelandic low has deepened during the recent decades while the Azores high intensified, and consequently, SWH extremes have increased in the northeast NA, accompanied by decreases of SWH extremes in the subtropical NA. Both SLP and H90 are highly significantly correlated with the NAO index. Similar results were also found for winter (JFM) 99th percentile wave heights. No significant trends of seasonal SWH extremes are found for the last century, though significant changes do exist in the last four decades; multi-decadal fluctuations are quite noticeable. These results are summarized in Figure 9. A more detailed description of these results can be found in Swail and Wang (2000).

5.4 Assessment of Homogeneity

While the NRA used the same numerical prediction scheme for the entire 40-year period, thus removing the bias associated with ever-changing operational models, there still remain probable biases due to increased observational quality and densities (Schmidt and von Storch, 1993). These are often referred to as "creeping inhomogeneities", and are potentially serious constraints to any attempt to

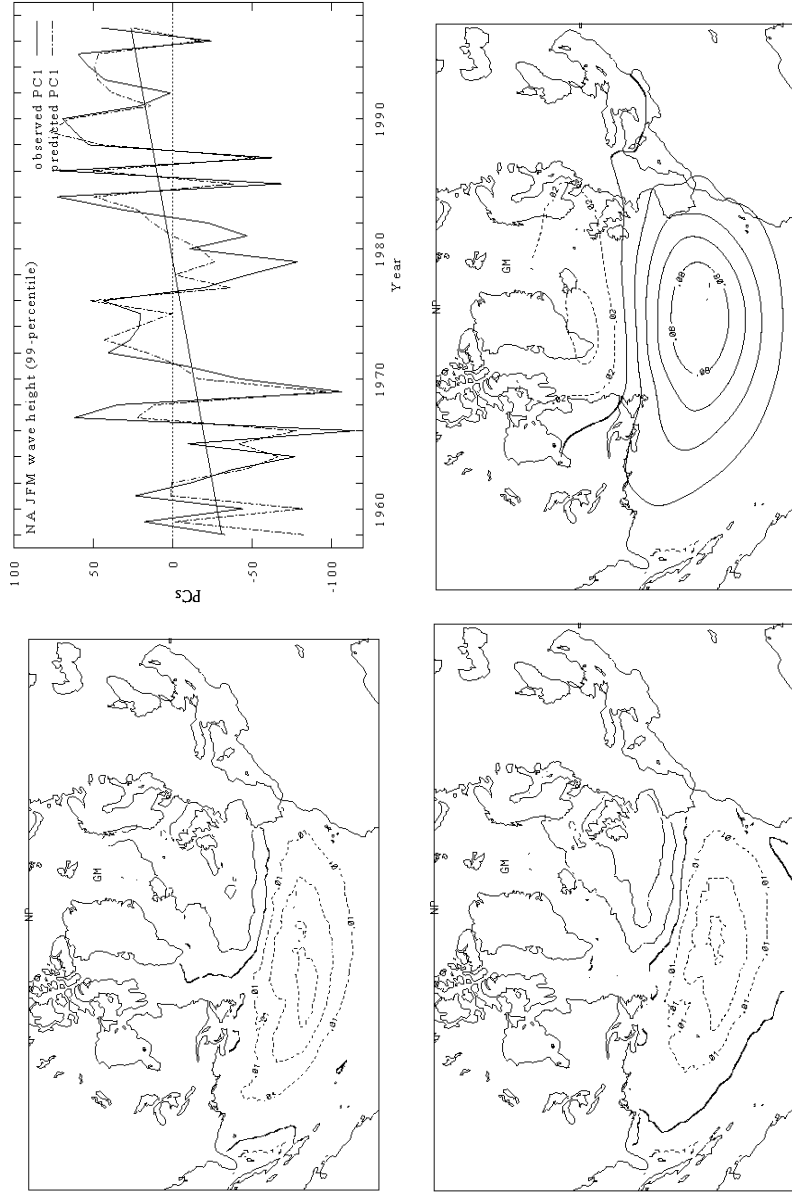


Figure 9. (top left, top right). First Empirical Orthogonal Function (EOF1) and first principal component (PC1) of winter (JFM) seasonal significant wave height extremes (H_{99}). The observed and predicted PC1s are PC1s of the numerical and statistical reconstruction, respectively. The trends shown were estimated from the numerical PC1. The contour interval is 0.01 m; solid, bold and dashed lines are positive, zero and negative contours, respectively. (bottom left, bottom right). The best predicted mode of winter seasonal 99-percentiles of significant wave height (H_{99}) in the North Atlantic and the associated predictor (SLP) mode, respectively. In the 1958-1997 period, both the predictor and predictand time series (SLP-T1 and H99-T1; normalized) have a significant increasing trend at 95% confidence level.

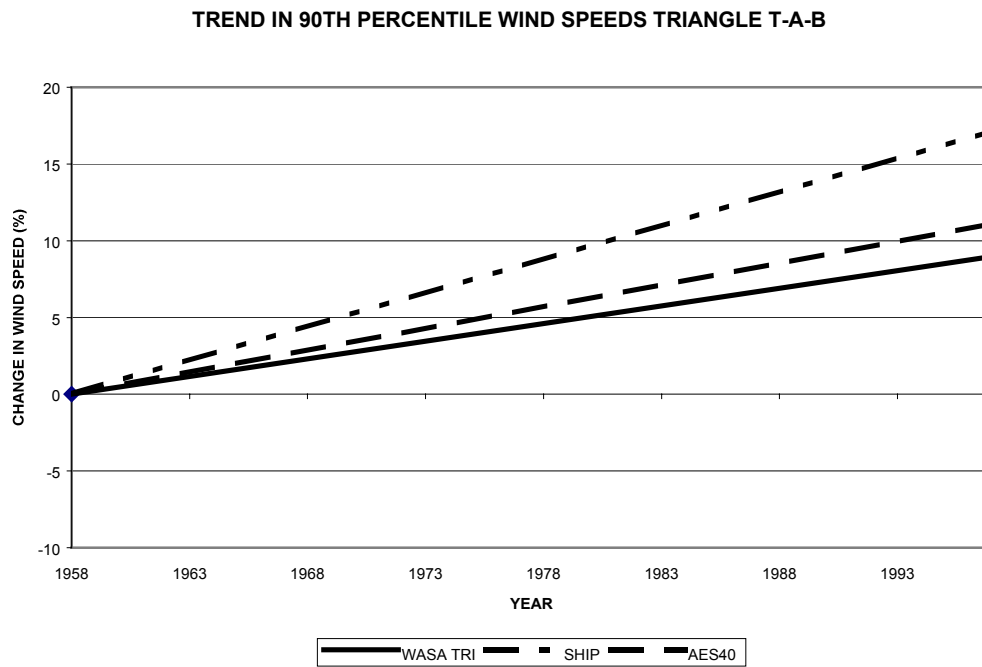
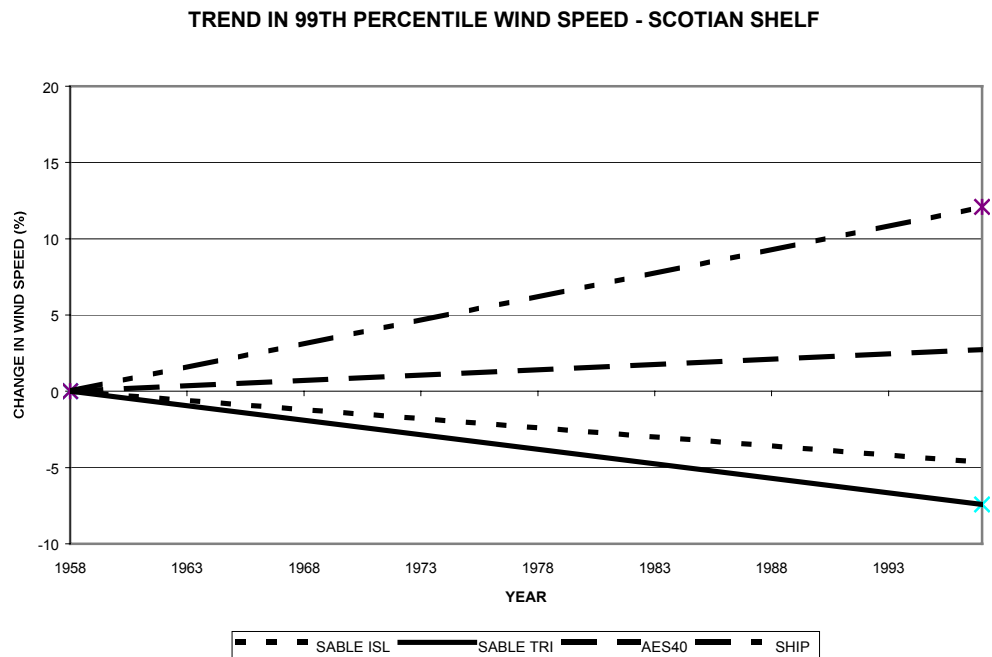


Figure 10. Trends in AES40 wind speeds and corresponding point trends expressed as the inferred percent change in 99th (lower panel 90th) percentile wind speed over the period 1958-1997 for the Sable Island area (upper) and the WASA triangle Thorshavn-Aberdeen-Bergen (lower)

derive long-term trends. Therefore, we would like to verify the trend analyses derived from the hindcast against some long time histories of homogeneous measured data at selected points. Unfortunately, there are very few such locations in the global ocean.

One location for which we do have reasonably homogeneous wind measurements over the 40-year period is at Sable Island, just off the east coast of Canada. We are also able to analyze the surface atmospheric pressure record from Sable Island, along with records from two other sites in Nova Scotia (Halifax, Sydney), to compute pressure triangle wind records. As shown by Schmidt and von Storch (1993), the pressure triangle winds are likely the least biased wind estimator available, since inhomogeneities in pressure records are much less than for most atmospheric variables.

Figure 10 shows the trends for the Sable Island area from the AES40 hindcast, Sable Island and the pressure triangle. In both the Sable Island measurements and the triangle winds the trends in the percentiles are decreasing; the magnitude of the decreasing trend is comparable in both analyses, with the triangle wind trend being slightly more negative. The hindcast wind speed trend shows a near-zero, but very slightly positive trend. This likely indicates an inhomogeneity introduced into the NRA winds. The AES40 trends should be a reasonable indication of the intangible creeping inhomogeneities in the reanalysis process, such as increased data density, since the other sources such as changing anemometer heights have been mostly removed. Figure 10 also shows the trends from Comprehensive Ocean-Atmosphere Data Set (COADS) ship observations. These wind speeds have been corrected where possible following the approach of Cardone *et al.* (1990). However, there remains a strong positive trend in wind speeds, particularly at the higher percentiles. Based on the Sable Island and triangle winds, this trend is likely spurious, indicating that even these methods are unable to remove all of the artificial trend introduced by changing observational procedures on ships.

A second area for which “ground truth” information is available for trends is off the Norwegian coast. WASA (1998) computed winds from two pressure triangles: (1) T-B-M (Thorshavn-Bergen-Mike (OWS)); and (2) T-A-B (Thorshavn-Aberdeen-Bergen). Figure 10 shows the comparative results of the hindcast and the T-A-B triangle. In this area both trends are strongly positive, the hindcast winds being slightly more positive than the triangles. This indicates that the hindcast trends are reasonable, but

probably slightly too high, or a good upper bound on real trends. Trends from adjusted ships in these areas similarly show too-strong increases in wind speed, especially in the higher percentiles. Results from the T-B-M triangle (not shown) were similar.

6. SUMMARY

This study describes the first engineering-quality 40-year wind and wave hindcast produced for the entire North Atlantic Ocean using a long term, consistent wind field forcing based on the NCEP re-analysis. The NRA surface wind fields have been kinematically reanalyzed to account for differences in wind observations, to reproduce small-scale features such as tropical storms, and to reduce the inherent low bias in extreme extratropical storms due to the limited grid resolution in the NRA wind fields. The wind fields are used to drive a 3rd generation wave model on a fine mesh grid covering the entire North Atlantic Ocean. The output from the wave model, consisting of 17 different fields is archived at 6-hour intervals at each grid location; 2-D wave spectra are archived every 6 hours at 233 grid points covering the entire basin, but particularly along the continental margins.

In situ and satellite observations have been used to evaluate the wind and wave hindcast. The hindcast compares well against the available buoy, platform, ocean weather ship and satellite measurements in all parts of the North Atlantic, not only in terms of bias and scatter, but over the entire frequency distribution out to and beyond the 99th percentiles of both winds and waves. Comparisons of *in situ* data over the full 1958-1997 period show that the hindcast has remained consistent with the observations. The wind and wave data are considered to be of sufficiently high quality to be used in the analysis of long return period statistics, and other engineering applications.

Extremal analysis was performed for the entire basin. Highest winds and waves are shown to occur over the North East Atlantic west of the United Kingdom and south of Iceland.

The trend analysis showed statistically significant areas of both increasing and decreasing winds and waves. The increasing trend in the North East Atlantic and decreasing trend in the Central North Atlantic are particularly well defined and consistent with changes reported in previous studies, which were linked to reported changes in the North Atlantic Oscillation. The apparent creeping inhomogeneities in the NRA winds highlight the need for additional investigation of the sources and magnitudes of the

inhomogeneities, by comparing the results of this (and subsequent) hindcasts to other long-term homogeneous data sets such as pressure triangles.

7. REFERENCES

- Borgman, L.E. 1973. Probabilities for the highest wave in a hurricane. *J. Waterways, Harbors and Coastal Engineering Div.*, ASCE, 185-207.
- Cardone, V.J., A.T. Cox, J.A. Greenwood, and E.F. Thompson, 1994. *Upgrade of tropical cyclone Surface wind field model*. U.S. Corps of Engineers Misc. Paper CERC-94-14.
- Cardone, V.J., H.C. Graber, R.E. Jensen, S. Hasselmann, and M.J. Caruso, 1995. *In search of the true surface wind field in SWADE IOP-1: ocean wave modeling perspective*. The Global Ocean Atmosphere System, **3**, 107-150.
- Cardone, V.J., J.G. Greenwood and M.A. Cane, 1990. *On trends in historical marine wind data*. *J. Climate*, **3**, 113-127.
- Cardone, V.J., R.E. Jensen, D.T. Resio, V.R. Swail and A.T. Cox, 1996. *Evaluation of Contemporary Ocean Wave Models in Rare Extreme Events: "Halloween Storm of October, 1991; "Storm of the Century" of March, 1993."* *J. Atmos. Ocean. Tech.*, **13**, 1, 198-230.
- Cotton, P.D., and D.J.T. Carter, 1994. *Cross calibration of TOPEX, ERS-1, and Geosat wave heights*. *J. of Geophysical Research*, **99**, C12, 25,025-25,033.
- Cox, A.T., and V.R. Swail, 2000. *A global wave hindcast over the period 1958-1997: validation and climate assessment*. *J. of Geophys. Res.*, (in press).
- Cox, A.T., J.A. Greenwood, V.J. Cardone and V.R. Swail, 1995. *An interactive objective kinematic analysis system*. Proceedings 4th International Workshop on Wave Hindcasting and Forecasting, October 16-20, 1995, Banff, Alberta, p. 109-118.
- Forristall, G.Z. 1978. *On the statistical distribution of wave heights in a storm*. *J. of Geophys. Res.*, **83**, 2353-2358.
- Forristall, G.Z. and J. A. Greenwood, 1998. *Directional spreading of measured and hindcasted wave spectra*. Proc. 5th International Workshop on Wave Hindcasting and Forecasting, Melbourne, FL, January 26-30, 1998.
- Greenwood, J.A., V.J. Cardone and L.M. Lawson, 1985. *Intercomparison test version of the SAIL wave model*. Ocean Wave Modelling, the SWAMP Group, Plenum Press, 221-233.
- Gumbel, E.J. 1958. *Statistics of Extremes*. Columbia University Press, New York, 375 pp.
- Haring, R.E., A.R. Osborne, and L.P. Spencer. 1976. *Extreme wave parameters based on continental shelf storm wave records*. Proceedings of the 15th Coastal Engineering Conference, Honolulu, July 11-17, 1976.
- Kalnay, E., et al, 1996. *The NCEP/NCAR 40-Year reanalysis project*. *Bull. Amer. Meteor. Soc.*, **77**, 3, 437-471.
- Khandekar, M.L., R. Lalbeharry and V.J. Cardone, 1994. *The Performance of the Canadian Spectral Ocean Wave Model (CSOWM) During the Grand Banks ERS-1 SAR Wave Spectra Validation Experiment*. *Atmosphere-Ocean*, **32**, 1, 31-60.
- Powell, M.D., and P.G. Black, 1989. *The relationship of hurricane reconnaissance flight-level wind measured by NOAA's oceanic platforms*. 6th National Conference on Wind Engineering, March 7-10, 1989.
- Schmidt, H. and H. von Storch, 1993. German Bight storms analyzed. *Nature*: **365**:791.
- Snyder, R., F.W. Dobson, J.A. Elliott and R.B. Long, 1981. *Array measurements of atmospheric pressure fluctuations above surface gravity waves*. *J. Fluid Mech.*, **102**, 1-59.
- Stutz, R.J., S.J. Lubker, J.D. Hiscox, S.D. Woodruff, R.L. Jenne, D.H. Joseph, P.M. Steurer, and J.D. Elms, 1985. *Comprehensive Ocean-Atmosphere Data Set Release 1*. NOAA Environmental Research Laboratories, Boulder, Colo., 268 pp. (NTIS PB86-105723).
- Swail, V.R. and A.T. Cox, 2000. *On the use of NCEP/NCAR reanalysis surface marine wind fields for a long term North Atlantic wave hindcast*. *J. Atmos. Ocean. Technol.*, **17**, 532-545.
- Swail, V.R. and X.L. Wang, 2000. Trends of Atlantic wave extremes as simulated in a 40-year wave hindcast using kinematically reanalyzed wind fields. Submitted to *J. Climate*.
- Swail, V.R., M. Parsons, B.T. Callahan and V.J. Cardone, 1995. *A revised extreme wave climatology for the east coast of Canada*. Proceedings 4th International Workshop on Wave Hindcasting and Forecasting, October 16-20, 1995, Banff, Alberta, p. 81-91.
- Swail, V.R., V.J. Cardone and A.T. Cox, 1998. *A Long Term North Atlantic Wave Hindcast*. Proc. 5th International Workshop on Wave Hindcasting and Forecasting, Melbourne, FL, January 26-30, 1998.
- Thompson, E.F., and V.J. Cardone, 1996. *Practical modeling of hurricane surface wind fields*. *Journal of Waterway, Port, Coastal, and Ocean Engineering*, July/August 1996, pp. 195-205.

- Walsh, J.E., and C.M. Johnson, 1979. *An analysis of Arctic sea ice fluctuations, 1953-1977*. J. Phys. Ocean., **9**, 580-591.
- WAMDI Group, 1988. *The WAM model - a third generation ocean wave prediction model*. J. Phys. Ocean. **18**: 1775-1810.
- Wang, X.L., F.W. Zwiers and H. von Storch, 2000. Using Redundancy analysis to improve dynamic seasonal mean 500 hPa geopotential forecasts. Submitted to J. Climate.
- WASA Group, 1998. *Changing waves and storms in the Northeast Atlantic?* Bull. AMS., **79**(5), 741-760.
- Wu, J., 1982. *Wind-stress coefficients over the sea surface from breeze to hurricane*. J. Geophys. Res., **87**, 9704-9706.